

Design of Novel FLT-3 Inhibitors Based on Dual-Layer 3D-QSAR Model and Fragment-Based Compounds *in Silico*

Kuei-Chung Shih,^{†,▽} Chun-Yuan Lin,^{‡,§,▽} Hsiao-Chieh Chi,[†] Chrong-Shiong Hwang,^{||} Ting-Shou Chen,^{||} Chuan-Yi Tang,^{*,†,⊥} and Nai-Wan Hsiao^{*,#}

[†]Department of Computer Science, National Tsing Hua University, Hsinchu 30013, Taiwan

[‡]Department of Computer Science and Information Engineering, Chang Gung University, Taoyuan 33302, Taiwan

[§]Research Center for Emerging Viral Infections, Chang Gung University, Taoyuan 33302, Taiwan

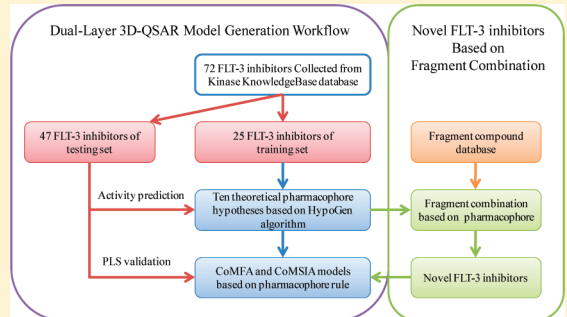
^{||}Biomedical Technology and Device Research Laboratories, Industrial Technology Research Institute, Chutung, Hsinchu, 31040, Taiwan

[⊥]Department of Computer Science and Information Engineering, Providence University, Taichung 43301, Taiwan

^{*}Institute of Biotechnology, National Changhua University of Education, Changhua 50007, Taiwan

Supporting Information

ABSTRACT: FMS-like tyrosine kinase 3 (FLT-3) is strongly correlated with acute myeloid leukemia, but no FLT-3-inhibitor cocomplex structure is available to assist the design of therapeutic inhibitors. Hence, we propose a dual-layer 3D-QSAR model for FLT-3 that integrates the pharmacophore, CoMFA, and CoMSIA. We then coupled the model with the fragment-based design strategy to identify novel FLT-3 inhibitors. In the first layer, the previously established model, Hypo02, was evaluated in terms of its correlation coefficient (r), RMS, cost difference, and configuration cost, with values of 0.930, 1.24, 106.45, and 16.44, respectively. Moreover, Fischer's cross-validation test of data generated by Hypo02 yielded a 98% confidence level, and the validation of the testing set yielded a best r value of 0.87. The features of Hypo02 were separated into two parts and then used to screen the MiniMaybridge fragment compound database. Nine novel FLT-3 inhibitors were generated in this layer. In the second layer, Hypo02 was subjected to an alignment rule to generate CoMFA- and CoMSIA-based models, for which the partial least-squares validation method was utilized. The values of q^2 , r^2 , and predictive r^2 were 0.58, 0.98, and 0.76, respectively, derived from the CoMFA model with steric and electrostatic fields. The CoMSIA model with five different fields yielded values of 0.54, 0.97, and 0.76 for q^2 , r^2 , and predictive r^2 , respectively. The CoMFA and CoMSIA models were used to constrain 3D structures of the nine novel FLT-3 inhibitors. This dual-layer 3D-QSAR model constitutes a valuable tool to easily and quickly screen and optimize novel potential FLT-3 inhibitors for the treatment of acute myeloid leukemia.



INTRODUCTION

Receptor tyrosine kinases (RTKs) are a large family of transmembrane receptors with diverse biological activities. At least 19 subfamilies of RTKs have been identified, such as the platelet-derived growth factor receptor (PDGFR) subfamily (type III). Members of this subfamily include PDGFR α , PDGFR β , colony stimulating factor 1 receptor, FMS-like tyrosine kinase 3 (FLT-3), and c-KIT, which are believed to promote angiogenesis and tumor cell proliferation. The constitutive activation of FLT-3 by different mutations or internal tandem duplication is directly associated with acute myeloid leukemia (AML). FLT-3 is overexpressed on blasts in most AML patients, and about 30% of AML patients express different types of FLT-3 mutants. The important role played by FLT-3 in blast survival and proliferation, and the overexpression in most AML patients, suggests it as an attractive therapeutic target.^{1–5}

Small-molecule inhibitors of FLT-3 have been postulated as a viable therapy for AML. Although no FLT-3 inhibitors have yet been approved for treatment of AML, several inhibitors are in clinical trials or under development (Figure 1). Sunitinib (Sutent)⁶ is approved for the treatment of both renal cell carcinomas and gastrointestinal stromal tumors; it inhibits PDGFR, vascular endothelial growth factor receptor (VEGFR), c-KIT, and FLT-3 in various cancer cell lines. Tandutinib (MLN-518)⁷ inhibits the autophosphorylation of FLT-3, c-KIT, and PDGFR, thereby inhibiting cellular proliferation and inducing apoptosis. Midostaurin (PKC-412)⁸ inhibits protein kinase C α (PKC α), VEGFR-2, c-KIT, PDGFR, and FLT-3, which may disrupt the cell cycle, inhibit proliferation, cause apoptosis, and inhibit angiogenesis in susceptible tumors.

Received: June 23, 2011

Published: December 5, 2011



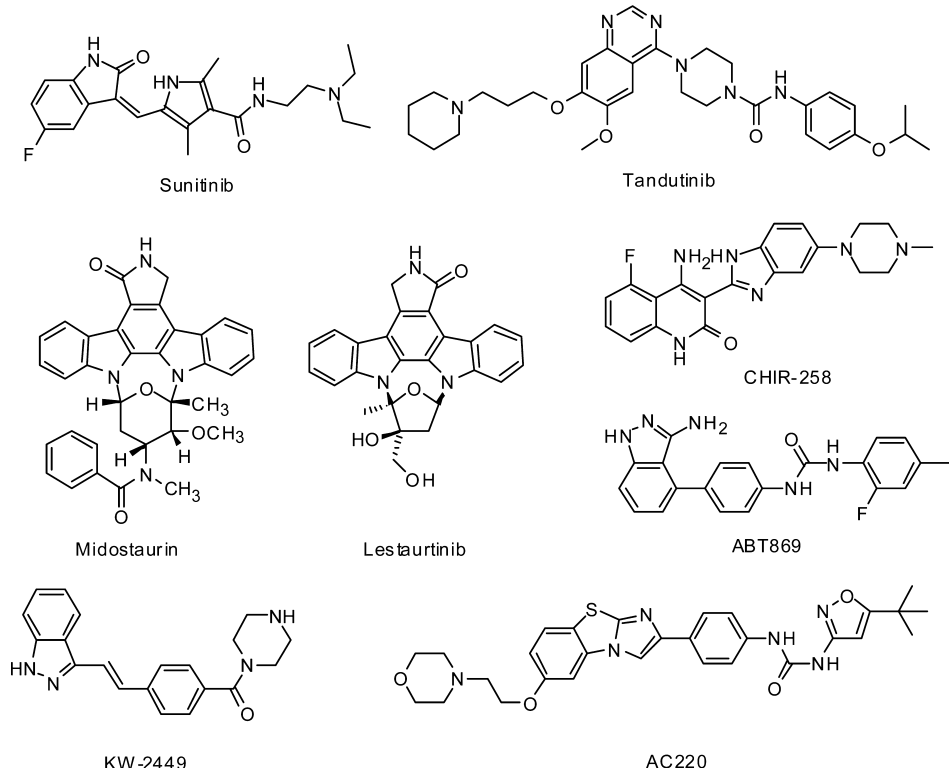


Figure 1. Structures of known FLT-3 inhibitors.

Lestaurtinib (CEP-701)⁹ is an orally active small-molecule inhibitor of several RTKs, including TrkA, TrkB, and TrkC, and it inhibits the activity of wild-type FLT-3. CHIR-258¹⁰ is an orally active and multitargeted small molecule with potent activity against FLT-3 and RTKs of types III, IV, and V, which are involved in endothelial and tumor cell proliferation in animal models of AML. ABT869¹¹ is an orally administered, potent, and specific inhibitor of all VEGFRs and PDGFRs, including FLT-3 and c-KIT. KW-2449,¹² a multikinase inhibitor of FLT-3, ABL, ABL-T315I, and Aurora, suppresses the growth of leukemia cells carrying FLT-3 mutations. AC220,¹³ a highly potent and selective inhibitor of FLT-3, shows low-nanomolar potency in both biochemical and cellular assays and also is orally effective in a xenographic animal model.

For structure-based drug design, a known structure of the target protein and the inhibitor binding site are needed. In the two FLT-3 structures that have been published, however, one comprises the cytosolic domain alone¹⁴ (PDB code 1RJB), which is usually where a kinase inhibitor would bind, and the other structure, published just recently¹⁵ (PDB code 3QS9), comprises the extracellular domain of FLT-3. This is a cocomplex structure between FLT-3 and its ligand, FL, however, and this binding interface is not the usual site at which kinase inhibitors bind. Thus, the structure cannot be used as the starting point for structure-based drug design. According to the above information and the fact that there is no available cocomplex structure between FLT-3 and any of its inhibitors, it is necessary to establish a model for rational drug design. Hence, FLT-3 was chosen as a target to combine pharmacophore hypotheses^{16–22} with comparative molecular field analysis^{23–32} (CoMFA) and comparative molecular similarity index analysis^{25–33} (CoMSIA) models to further discover potential FLT-3 inhibitors for treatment of AML.

Pharmacophore methodology is useful for searching large databases of compounds during the initial phase of drug discovery. This approach has two major problems, however; one is that the number of pharmacophore features is restricted to a maximum of five, and another is that the pharmacophore approach can only identify suitable inhibitors and cannot constrain the three-dimensional (3D) space of inhibitor structures. The advantages of CoMFA and CoMSIA methodologies are their abilities to rapidly predict candidate inhibitors, to constrain the 3D space of inhibitor structures, and to easily utilize contour information to optimize the inhibitor structure. However, one of the shortcomings of the CoMFA and CoMSIA methodologies is that both need a common substructure of inhibitors to align and generate models, and this has rendered these two methodologies unsuitable for searching compound databases.

Our present study had two objectives, namely, to address the disadvantages of these three methodologies and to develop a new means of using the methodologies to design novel FLT-3 inhibitors. We integrated the pharmacophore, CoMFA, and CoMSIA models to establish a dual-layer 3D-QSAR model that was derived from the same FLT-3 inhibitors as a training set. These models can be used (i) in different applications of the drug design progress, such as virtual screening, (ii) to predict the bioactivity and limit 3D space of candidate FLT-3 inhibitors, and (iii) to directly modify and optimize the chemical structure of the target compound in 3D space before synthesis.

MATERIALS AND 3D-QSAR MODELING METHODS

Biological Data Collection. The structure–activity relationship (SAR) information for FLT-3 inhibitors was collected from the Kinase KnowledgeBase database (Eidogen-Sertanty Inc.). According to the structural variations and chemical

differences in kinase-inhibitor activity, we used 72 known FLT-3 inhibitors to generate and validate the pharmacophore, CoMFA, and CoMSIA models. Dividing training- and testing-set inhibitors is a crucial step in generating and testing a dual-layer 3D-QSAR model. We thus adhered to the following four rules to divide the 72 known FLT-3 inhibitors into a training set, and the remaining inhibitors served as a testing set: (i) At a minimum, 16 diverse compounds were selected to ensure that statistical significance could be assessed. (ii) The biological activity data associated with the compounds spanned at least 4 orders of magnitude. (iii) Clear and concise information on the selected compounds was obtained to avoid any redundancy or bias in terms of structural features and activity range. (iv) The most active and least active compounds were included in the training set. On the basis of these rules, the 72 inhibitors were divided into the training set (25 inhibitor structures shown in Figure 2) and testing set (47 inhibitor structures shown in Supporting Information Figures S1–S3). The biological activity of all inhibitors, represented as IC_{50} (nanomolar), was divided into three groups: highly active ($IC_{50} < 100$ nM), moderately active (100 nM $\leq IC_{50} \leq 1000$ nM), and inactive ($IC_{50} > 1000$ nM).

Dual-Layer 3D-QSAR Modeling. Three 3D-QSAR models, pharmacophore, CoMFA, and CoMSIA, were utilized in this study. The pharmacophore hypothesis was calculated using the program Discovery Studio 2.1 (Accelrys) with data in the form of IC_{50} values, and the CoMFA and CoMSIA models were calculated using the program Sybyl-X 1.0 (Tripos) with data in the form of pIC_{50} values. We first established 10 theoretical pharmacophore hypotheses and then used the best hypothesis to align inhibitor structures to establish the CoMFA and CoMSIA models. Figure 3 presents a workflow with which the dual-layer 3D-QSAR models were generated. To generate the first layer, the 10 theoretical pharmacophore hypotheses were established on the basis of the training-set inhibitors, and then the testing-set inhibitors were used to validate the prediction ability of the 10 hypotheses. To generate the second layer, the best hypothesis generated from the first layer was subjected to the alignment rule and search interface to generate the CoMFA and CoMSIA models and to search various compound databases. The models generated in the second layer were used to restrict the 3D space and predict the biological activity of both known and candidate FLT-3 inhibitors. The partial least-squares (PLS) validation with the testing-set inhibitors was used to validate the prediction ability of models.

Pharmacophore Generation. Pharmacophore hypotheses were generated using the “3D-QSAR Pharmacophore Generation” protocol in the HypoGen algorithm.³⁴ For the input data, IC_{50} values of the 25 training-set inhibitors are shown in Table 1. On the basis of the program settings, all of the training-set inhibitor conformations were generated using the “BEST” generation option based on CHARMm-like force field³⁵ parameters. A maximum of 255 conformations were generated for each inhibitor. In addition, a conformational space was constrained to a threshold (20 kcal/mol) of the global minimum energy. Two features, hydrogen bond acceptor and hydrophobic, were set for the pharmacophore generation during the initial phase. The minimum and maximum counts for each feature were set to 0 and 3, respectively. All other parameters were set to default values.

Alignment Rule for CoMFA and CoMSIA Models. The alignment rule for CoMFA and CoMSIA models was based on chemical characteristics of the ligand-based pharmacophore.

The training set for establishing the CoMFA and CoMSIA models was the same as that for the pharmacophore generation. The 255 3D conformations of each inhibitor were generated by the “BEST” option based on CHARMm-like force field parameters. All conformations were aligned to a 3D geometric model, as performed by the “Ligand Pharmacophore Mapping” protocol in Discovery Studio 2.1. This aligned result was used to assess the performance the CoMFA and CoMSIA models.

Generation of CoMFA and CoMSIA Models. Gasteiger–Hückel charges were assigned to each of the 3D inhibitor structures mentioned above. The CoMFA model was performed on the basis of the Sybyl-X 1.0 (Tripos) standard field and an sp^3 -hybridized carbon atom with a +1 charge set as a probe. In addition, the steric (Lennard-Jones potential) and electrostatic (Coulombic potential) fields were calculated on each grid point, and the energy cutoff value was set to 30 kcal/mol. The CoMFA and CoMSIA models shared a common probe atom, aligned structure, and training set; however, the five fields, namely steric, electrostatic, hydrophobic, hydrogen bond acceptor, and hydrogen bond donor, were all calculated on the basis of an attenuation factor value of 0.3 in the CoMSIA model. The distance dependence function between the probe and inhibitor atom was set via the Gaussian type of CoMSIA model.

■ VALIDATION METHODS OF DUAL-LAYER 3D-QSAR MODEL

The quality of the 10 pharmacophore hypotheses was estimated by (i) a cost function and (ii) Fischer’s cross-validation test (Fischer’s test). The CoMFA and CoMSIA models were validated on the basis of the PLS analysis.

Cost Function Analysis. The success of each pharmacophore hypothesis was determined by two important theoretical cost calculations (in units of “bits”) when performing the “3D-QSAR Pharmacophore Generation” protocol in Discovery Studio 2.1. One is the fixed cost, which represents the simplest model that fits all data perfectly. The other one is the null cost, which represents the highest cost of a model with no correlation. The activity predicted by the null hypothesis is the average activity of training-set inhibitors. A pharmacophore hypothesis was found to be significant when the difference between the null and fixed costs was large (i.e., $>X$ [bits]). Specifically, a good pharmacophore hypothesis should satisfy the following conditions. If the difference between the fixed and null costs is >70 bits, there is a $>90\%$ chance that the actual and predicted activity data will correlate.³⁴ The total cost must, however, be close to the fixed cost for a perfect model. In addition, the configuration cost must be <17 bits.

Fischer’s Cross-Validation Test. We also applied Fischer’s randomization test to cross-validate the functions in the “3D-QSAR Pharmacophore Generation” protocol.³⁶ The affinity for the active training-set compounds was reshuffled and then used to generate the pharmacophore hypothesis by taking the same features and parameters used to develop the original pharmacophore. To achieve a confidence level of 98%, the procedure was performed 49 times according to the following equation:

$$\text{confidence, } 98\% = [1 - (1 + 0)/(x + 1)] \times 100\% \quad (1)$$

where x is the number of times the procedure was carried out.

PLS Analysis for CoMFA and CoMSIA Models. The PLS³⁷ method was used to assess the validity of CoMFA and CoMSIA models, which indicated a linear relationship between the activity and computed fields. The filtering value column was

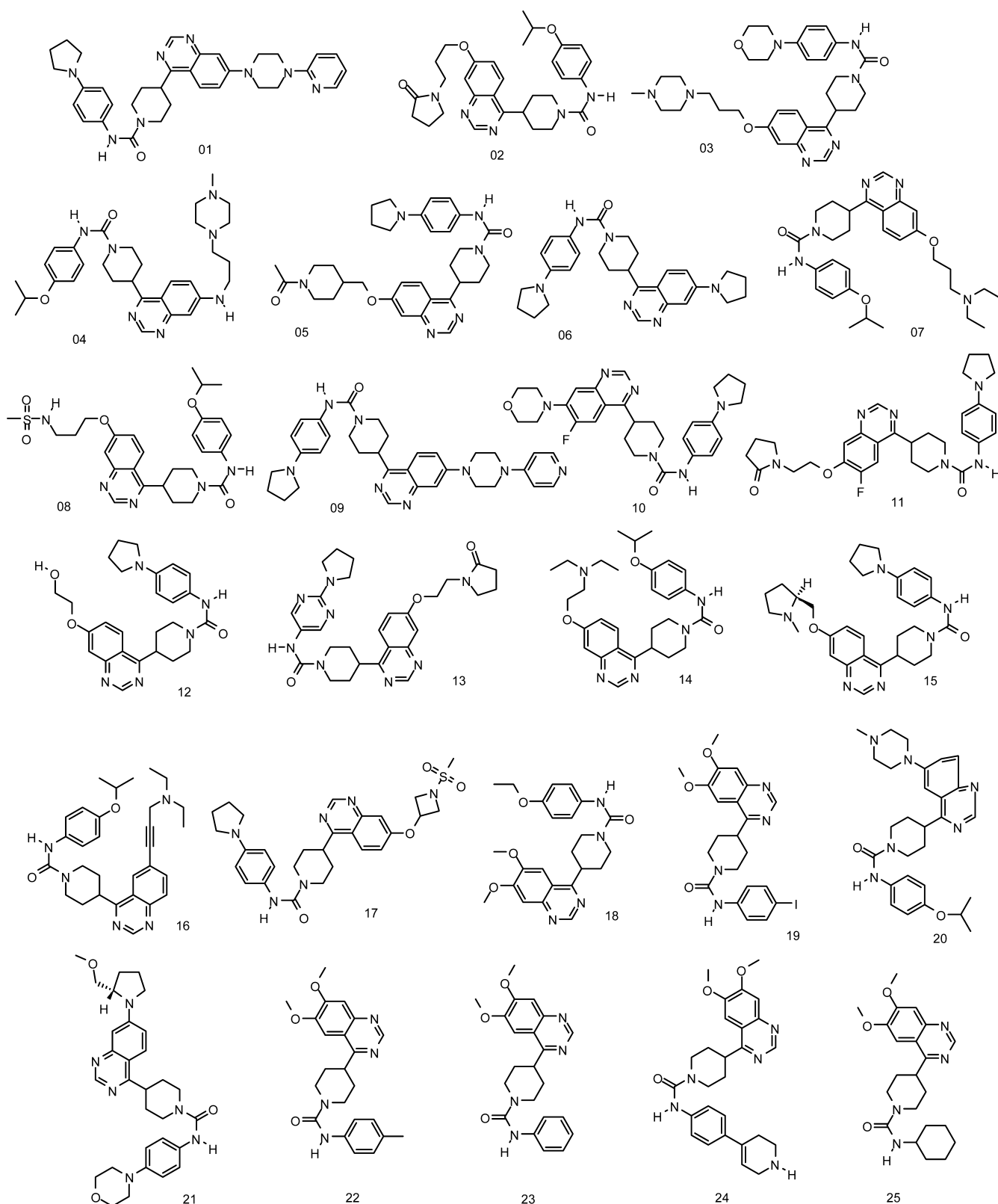


Figure 2. The 25 FLT-3 inhibitor structures of the training set that were used to generate dual-layer 3D-QSAR models.

set as a default value, 2.0. We also followed the leave-one-out method to determine the optimal number of components, and a coefficient q^2 was determined via the cross-validation analysis. Below, we describe the core process of the leave-one-out method. By removing one inhibitor from the training set and

manipulating a model established by the remaining training-set inhibitors, we could predict the activity of the removed inhibitor. When the coefficient r_{loo}^2 of the leave-one-out method was >0.5 , however, the optimal number of components that was considered for the calculation of the coefficient r^2 in the

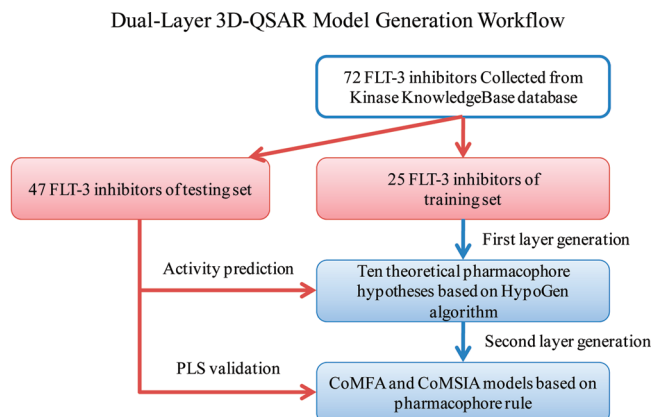


Figure 3. Workflow for the generation of dual-layer 3D-QSAR models.

Table 1. Actual and Predicted IC₅₀ Values (nM) of the Training-Set Inhibitors Based on Hypo02, CoMFA, and CoMSIA Models

no.	pharmacophore Hypo02			CoMFA and CoMSIA models		
	actual ^a IC ₅₀	predicted ^a IC ₅₀	error ^b	pIC ₅₀	predicted CoMFA	predicted CoMSIA
1	2	2.9	+1.4	8.70	8.60	8.78
2	3	4.5	+1.5	8.52	8.60	8.60
3	3	4.4	+1.5	8.52	8.45	8.66
4	5	7.7	+1.5	8.30	8.36	8.17
5	11	47	+4.2	7.96	7.78	7.72
6	17	66	+3.9	7.77	7.54	7.54
7	18	31	+1.7	7.74	7.89	7.67
8	19	65	+3.4	7.72	7.70	7.67
9	20	5.2	-3.9	7.70	7.72	7.81
10	21	50	+2.4	7.68	7.44	7.55
11	28	33	+1.2	7.55	7.65	7.49
12	32	51	+1.6	7.49	7.31	7.41
13	41	47	+1.1	7.39	7.56	7.57
14	47	15	+3.1	7.33	7.35	7.19
15	62	36	-1.7	7.20	7.35	7.30
16	72	52	-1.4	7.14	7.01	7.02
17	130	43	-3	6.89	7.09	7.09
18	150	82	-1.8	6.82	6.77	6.82
19	210	350	+1.7	6.68	6.65	6.40
20	436	270	-1.6	6.36	6.54	6.73
21	626	68	-9.2	6.20	6.21	6.26
22	1600	1600	-1	5.80	6.13	6.17
23	3700	6000	+1.6	5.43	5.30	5.38
24	10000	6000	-1.7	5	4.81	4.97
25	10000	6000	-1.7	5	5.09	4.96

^aScale: highly active (IC₅₀ < 50 nM), moderately active (100 nM ≤ IC₅₀ ≤ 1000 nM), and inactive (IC₅₀ > 1000 nM). ^b+: Predicted IC₅₀ greater than the actual IC₅₀. -: Predicted IC₅₀ lower than the actual IC₅₀.

noncross-validation analysis and q^2 in the cross-validation analysis could be derived. The CoMFA and CoMSIA models could correctly classify testing-set inhibitors as active or inactive. Equation 2 was used to calculate the coefficient of predictive r^2 (r_{pred}^2) on the basis of the testing set.

$$\text{predictive } r^2 = 1 - \frac{\text{PRESS}}{\text{SD}} \quad (2)$$

where SD is the sum of the squared deviations between the actual activity of the testing set and the mean activity of the

training set and PRESS is the sum of the squared deviations between the predicted and actual activities for each inhibitor in the testing set.

RESULTS

Pharmacophore Generation Results. Ten pharmacophore hypotheses were generated by using the training-set inhibitors, which took two features into consideration: hydrogen bond acceptor and hydrophobic. Table 2 presents information concerning the 10 hypotheses, termed Hypo01 to Hypo10. The null cost of the 10 hypotheses was 216.65 bits, whereas the fixed cost was 90.13 bits. Thus, the difference between null and fixed costs is 126.52 bits, indicating that all 10 hypotheses had high prediction ability. In addition, the configuration cost was 16.44 bits, which is within the allowed range (i.e., <17). According to the cost function analysis, the total cost of a good-quality pharmacophore hypothesis should be close to the fixed cost and much lower than the null cost. In our case, the highest total cost of the worst hypothesis, Hypo10, was 115.89 bits. The cost difference of Hypo10 was >70 bits. The correlation coefficient r of the 10 hypotheses ranged from 0.948 to 0.908.

One of the major methods used to evaluate the prediction ability of a pharmacophore hypothesis is to predict the activity of known inhibitors in the testing set and then classify them as active or inactive. In our study, we selected 47 inhibitors in the testing set. The predicted activities of the testing-set inhibitors were assessed by the 10 hypotheses. In general, a reasonable r value for testing-set validation (i.e., $r > 0.8$) was obtained from the linear regression of the predicted activity versus the actual activity. The best r value for the testing-set validation was 0.87, derived from Hypo02, thereby validating Hypo02 as a statistically reliable predictor of FLT-3 inhibitor activity (Table 2). Hypo02 contains one hydrogen bond acceptor feature and three hydrophobic features (Figure 4). Supporting Information Table S1 presents predicted activity values of testing-set inhibitors by Hypo02. Compared with the other Hypo models, Hypo02 had a superior ability to predict the actual activity of a FLT-3 inhibitor and thus was the best pharmacophore hypothesis for screening databases and determining the alignment rule for the CoMFA and CoMSIA models. Figure 4a and b present data for the most active (inhibitor 01) and least active (inhibitor 25) FLT-3 inhibitors, aligned in Hypo02.

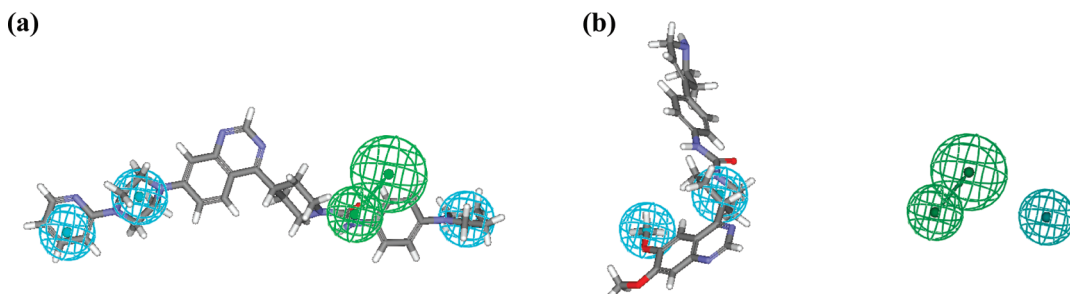
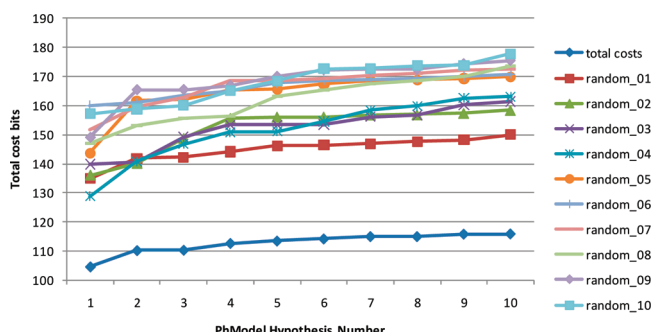
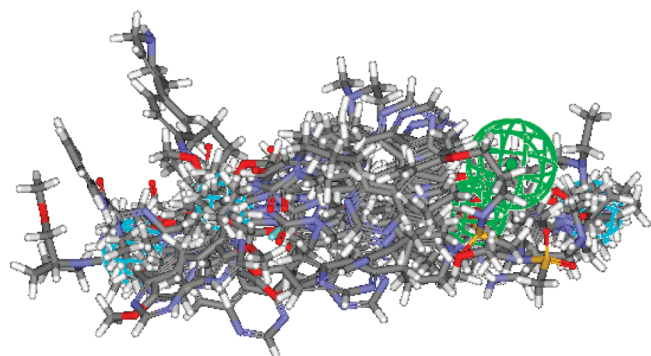
Pharmacophore Validation by Fischer's Test. Fischer's test was applied to validate the quality of the pharmacophore hypotheses. For Fischer's test, the IC₅₀ values of compounds were randomly reassigned to compounds in the training set; the program parameters of each randomized pharmacophore hypothesis were the same as those used to generate the original pharmacophore hypothesis, and this procedure was repeated 49 times. The total costs of the 10 original pharmacophore hypotheses were lower than that for any of the 49 randomization procedures, implying that the 10 hypotheses had a 98% confidence level with respect to the training set. Figure 5 presents the total costs from the hypotheses and the 10 lowest total costs from randomized results. As mentioned above, the training set could not be generated by using the randomized procedure.

Generation of the CoMFA and CoMSIA Models on the Basis of the Hypo02 Alignment Rule. By using the Hypo02-based alignment rule, the 25 FLT-3 inhibitors having IC₅₀ values ranging from 2 nM to 10000 nM were used to establish the CoMFA and CoMSIA models, as shown in Figure 6.

Table 2. Ten Pharmacophore Hypotheses Generated by the FLT-3 Training-Set Inhibitors

hypo no.	total cost	cost difference ^a	error cost	RMS deviation	training set (<i>r</i>)	testing set (<i>r</i>)	feature ^b
1	104.65	112	87.08	1.07	0.948	0.81	A* ² ,HY* ³
2	110.20	106.45	91.97	1.24	0.930	0.87	A, HY*³
3	110.33	106.32	92.76	1.27	0.927	0.81	A* ² ,HY* ³
4	112.64	104.01	95.07	1.34	0.918	0.80	A, HY* ³
5	113.46	103.19	95.88	1.36	0.915	0.76	A* ² ,HY* ²
6	114.17	102.48	96.44	1.38	0.913	0.76	A* ² ,HY* ²
7	114.97	101.68	96.30	1.37	0.914	0.80	A* ² ,HY* ²
8	114.98	101.67	97.39	1.40	0.909	0.80	A* ² ,HY* ²
9	115.81	100.84	97.69	1.41	0.908	0.80	A* ² ,HY* ³
10	115.89	100.76	97.65	1.41	0.908	0.80	A* ² ,HY* ³

^a(null cost – total cost), null cost = 216.65, fixed cost = 90.13, configuration cost = 16.44. All costs are in units of bits. ^bA, hydrogen bond acceptor; HY, hydrophobic.

**Figure 4.** Mapping Hypo02 for (a) the most active inhibitor 01 and (b) the least active inhibitor 25.**Figure 5.** Total cost (in bits) of the original pharmacophore hypotheses and randomized pharmacophore procedures with lowest costs.**Figure 6.** Alignment of FLT-3 training-set inhibitors by Hypo02 for the generation of the CoMFA and CoMSIA models.

These values were transformed to pIC_{50} (the negative logarithm of IC_{50} ; Table 1). The CoMFA model was calculated with steric and electrostatic fields. In the PLS analysis, a q^2

value of 0.58 and three optimal components were derived from the cross-validation method. The non-cross-validation analysis yielded an r^2 value of 0.98 with a standard error of estimate of 0.16 and an *F* ratio of 325.59. The steric and electrostatic fields comprised 0.49 and 0.51, respectively, of the relative contributions, as shown in Table 3. The steric and electrostatic contour maps of the CoMFA model are shown in Figures 7 and 8, respectively.

The CoMSIA model consisted of five fields that were derived from the steric, electrostatic, hydrophobic, hydrogen bond donor, and hydrogen bond acceptor. By combining these five fields, we established a model that had a cross-validation q^2 of 0.54 and three optimal components. The non-cross-validation analysis yielded an r^2 value of 0.97 with a standard error of estimate of 0.18 and *F* ratio of 256.24. The contributions of the steric, electrostatic, hydrophobic, hydrogen bond donor, and hydrogen bond acceptor fields were 0.18, 0.22, 0.20, 0.19, and 0.21, respectively (Table 3). The hydrophobic, hydrogen bond donor, and hydrogen bond acceptor contour maps of the CoMSIA model are shown in Figures 9–11, respectively.

In the CoMFA and CoMSIA model validations, we used the 47 testing-set inhibitors that were the same as those used for the pharmacophore validation above. On the basis of the testing set, predicted pIC_{50} values were calculated with the CoMFA and CoMSIA models. The predictive r^2 value was 0.76 for each of the CoMFA and CoMSIA models (Table 3), indicating that these models had good predictive power.

Contour Map Analysis of the CoMFA and CoMSIA Models. On the basis of the pharmacophore alignment of individual inhibitors, the CoMFA and CoMSIA models did not require a common inhibitor structure. The contour map can vividly display the aligned molecules having regions that are

Table 3. Summary Results for CoMFA and CoMSIA Models for Prediction of FLT-3 Inhibitors

parameters	q^2	NC ^b	r^2	SEE ^c	F-ratio	predictive r^2	contributions ^a				
							S	E	H	D	A
CoMFA	0.58	3	0.98	0.16	325.59	0.76	0.49	0.51			
CoMSIA	0.54	3	0.97	0.18	256.24	0.76	0.18	0.22	0.20	0.19	0.21

^aCoMFA and CoMSIA models with different field contributions such as S (steric), E (electrostatic), H (hydrophobic), D (hydrogen bond donor), A (hydrogen bond acceptor). ^bNC, number of components. ^cSEE, standard error of estimate.

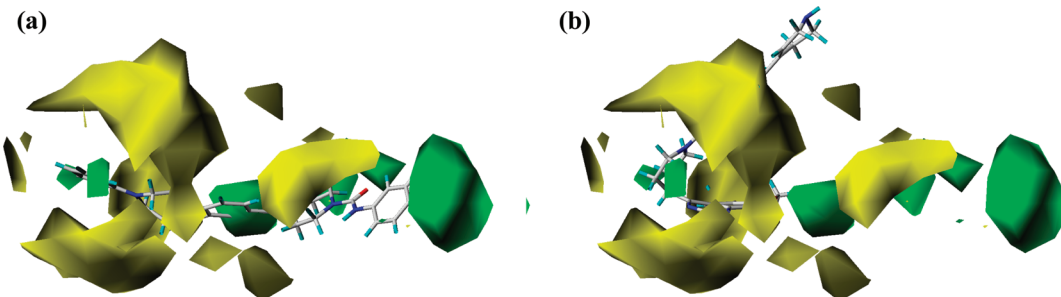


Figure 7. CoMFA steric STDEV*COEFF contour plots of (a) the most active inhibitor 01 and (b) the least active inhibitor 25, aligned on the basis of Hypo02. Sterically favored regions (contribution level, 80%) are represented by green contours. Sterically disfavored regions (contribution level, 20%) are represented by yellow contours.

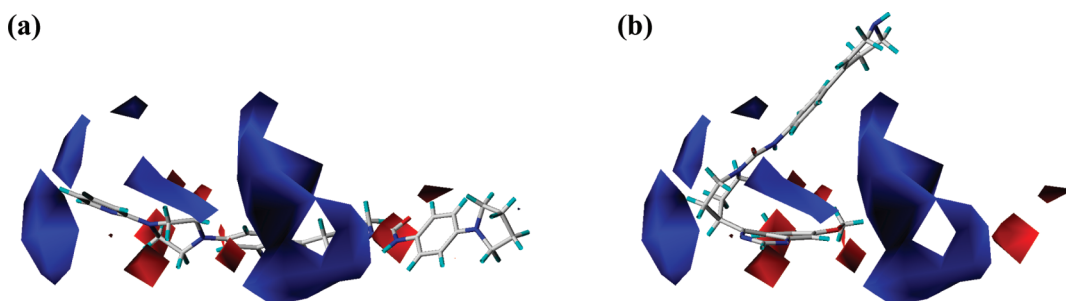


Figure 8. CoMFA electrostatic STDEV*COEFF contour plots of (a) the most active inhibitor 01 and (b) the least active inhibitor 25, aligned on the basis of Hypo02. Positive-charge areas (contribution level, 80%) are represented by blue contours. Negative-charge areas (contribution level, 20%) are represented by red contours.

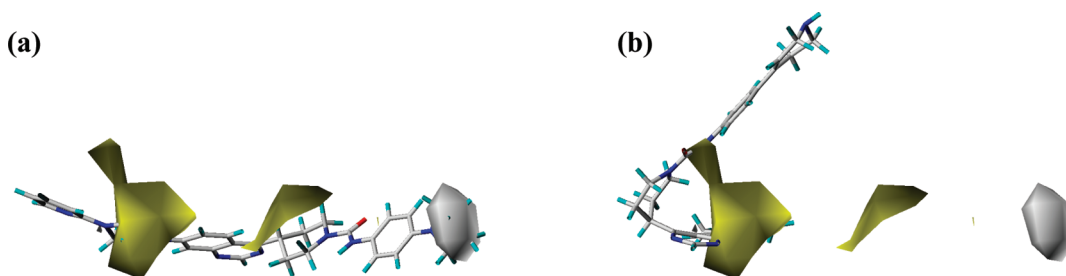


Figure 9. CoMSIA hydrophobic STDEV*COEFF contour plots of (a) the most active inhibitor 01 and (b) the least active inhibitor 25, aligned on the basis of Hypo02. Hydrophobic-favored regions (contribution level, 80%) are represented by yellow contours. Hydrophobic-disfavored regions (contribution level, 20%) are represented by white contours.

favored or disfavored for association with the binding site of FLT-3 in a 3D space.

The CoMFA and CoMSIA models could easily be used to describe the molecular weight range limitation for the inhibitors. In addition, these models could be used to optimize the inhibitor structure and identify potential analogs. The inhibitor 01 (the most active inhibitor) and inhibitor 25 (the least active inhibitor) were used as template structures (Figures 7–11). In Figure 7a and b, the green and yellow regions denote areas of steric tolerance and intolerance, respectively. The green contours

shown in Figure 7a are distributed uniformly. The conformation of inhibitor 01 is oriented to insert into the green contours, implying a sterically favored interaction. In Figure 7b, inhibitor 25 is oriented to insert into the yellow contours and does not make contact with any green contours. Therefore, the overlap of an inhibitor with sterically tolerant regions may imply a higher inhibitor activity. Inhibitors that come close to or actually contact the yellow contours would have decreased activity.

The electrostatic contour map clearly shows the distribution of positive and negative electrostatic regions (Figure 8).

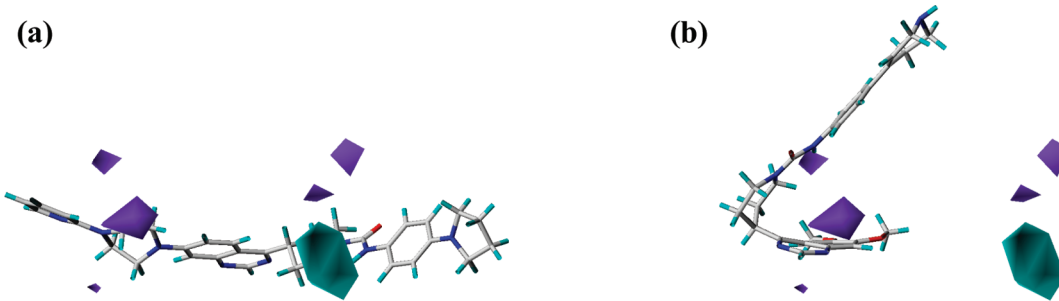


Figure 10. CoMSIA hydrogen bond donor STDEV*COEFF contour plots of (a) the most active inhibitor 01 and (b) the least active inhibitor 25, aligned on the basis of Hypo02. Hydrogen-bond-donor-favored regions (contribution level, 80%) are represented by cyan contours. Hydrogen-bond-donor-disfavored regions (contribution level, 20%) are represented by purple contours.

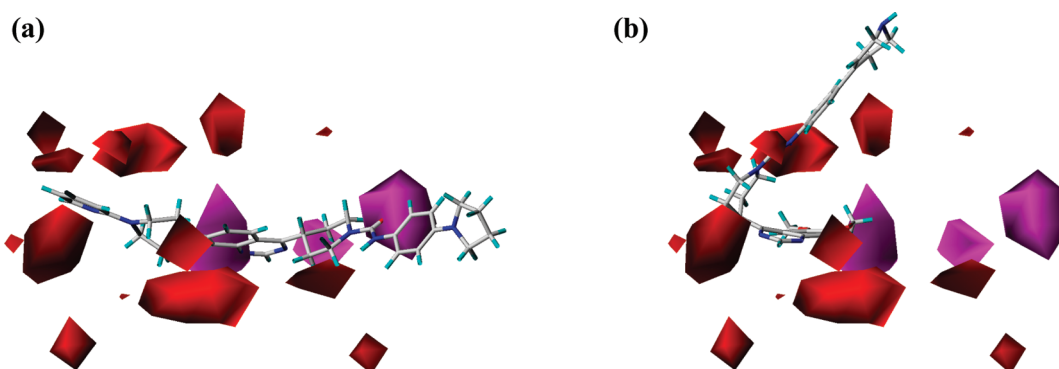


Figure 11. CoMSIA hydrogen bond acceptor STDEV*COEFF contour plots of (a) the most active inhibitor 01 and (b) the least active inhibitor 25, aligned on the basis of Hypo02. Hydrogen-bond-acceptor-favored regions (contribution level, 80%) are represented by magenta contours. Hydrogen-bond-acceptor-disfavored regions (contribution level, 20%) are represented by red contours.

In Figure 8a, the positive-charge areas are displayed as blue contours that are distributed in the *N*-methylpiperidine-1-carboxamide and pyridine of the inhibitor 01 structure. The red contours represent negative-charge areas. The conformation of inhibitor 25 is projected out of the blue contours (Figure 8b). The inhibitory capacity of the FLT-3 inhibitor increases with contour contact. Therefore, the more the conformation of a compound fits either positive or negative electrostatic contours, the more likely the compound would serve as a candidate inhibitor of FLT-3.

The hydrophobic-favored and -disfavored regions are clearly distributed (Figure 9). The hydrophobic-favored regions are displayed as yellow contours, and disfavored regions are displayed as white contours. The dimethylpiperazine and methylpiperidine groups of inhibitor 01 are close to the two yellow contours (Figure 9a). In Figure 9b, only the dimethoxyquinazoline group of inhibitor 25 is enclosed by a yellow contour. These results demonstrated that compounds for which the hydrophobic contours are maximized may constitute the most effective FLT-3 inhibitors.

The hydrogen bond donor-favored and -disfavored regions are represented by cyan and purple contours, respectively, in Figure 10. The main cyan contour surrounds the *N*-methylformamide group of inhibitor 01 (Figure 10a). No part of inhibitor 25 is within the hydrogen bond donor contour (Figure 10b). The cyan contour leads the increased activity of inhibitors for FLT-3.

The hydrogen bond acceptor contours of the CoMSIA model were clearly distributed and indicated favored and disfavored regions, as designated by magenta and red contours, respectively, in Figure 11. Three magenta contours surround

the electronegative atom. In Figure 11a, the middle of the inhibitor 01 structure is enclosed by three magenta contour regions. The formaldehyde group of inhibitor 01 is close to a magenta contour, and the quinazoline group is close to another magenta contour. In Figure 11b, the dimethoxyquinazoline group of inhibitor 25 is close to a magenta contour. Thus, the hydrogen-bond-acceptor-favored contour could lead to increased activity of a candidate FLT-3 inhibitor.

Design of Novel FLT-3 Inhibitors. On the basis of the above analysis, each inhibitor could be easily aligned using the pharmacophore hypothesis without any common structure, and each could be aligned with the contour analysis of CoMFA and CoMSIA models. The favored and disfavored contour information of the CoMFA and CoMSIA models clearly provides 3D space constraints, although more detailed chemical characteristics of 3D space are required. Therefore, we propose a fragment-based design strategy, as part of the dual-layer 3D-QSAR model generation, for design of novel FLT-3 inhibitors. In the first step, the features of Hypo02 were divided into two parts and then used to screen the MiniMaybridge fragment compound database and combine the structures. The first part has one hydrogen bond acceptor feature and one hydrophobic feature; the second part has two hydrophobic features. Figure 12 presents the workflow for the design of novel FLT-3 inhibitors based on a fragment-based design strategy with our dual-layer 3D-QSAR model. The first step is to combine the fragment compounds from the MiniMaybridge fragment compound database with the first-layer model (Hypo02). Nine novel FLT-3 inhibitors were generated in the first step. In the second step, the second-layer models (CoMFA and CoMSIA models based on the Hypo02 alignment rule) were

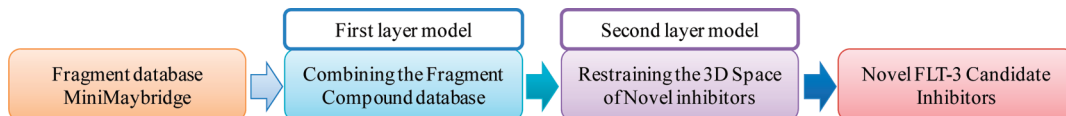


Figure 12. Workflow for the design of novel FLT-3 inhibitors based on the dual-layer 3D-QSAR model and fragment-based design strategy.

used to constrain the 3D space of nine novel FLT-3 inhibitors. The structures of these nine inhibitors are shown in Supporting Information Table S2, and their predicted biological activities are shown in Supporting Information Table S3.

We used steric contours of the CoMFA model and one of nine inhibitors, EnFrag-01 (Enumerate Fragments 01), as a template structure. In Figure 13, EnFrag01 is surrounded by

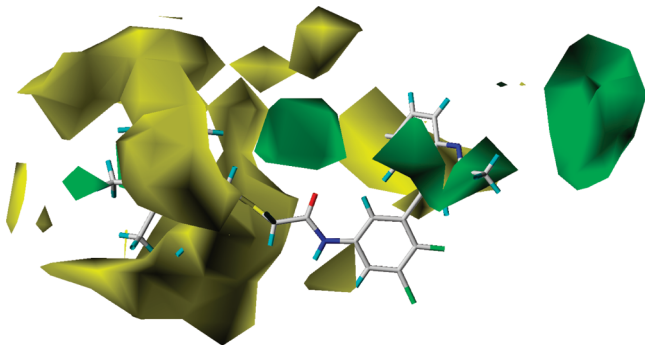


Figure 13. The novel FLT-3 inhibitor, EnFrag01, was constrained by steric contours of the CoMFA model.

contours of steric tolerance and intolerance. Only the 2-methylpyridine group makes contact with the tolerance contour. The dimethylsulfane and hexamethylbenzene groups are oriented to insert into intolerance contours. On the basis of the contour analysis, the inhibitory activity of a compound will be higher if the structure fits well within the tolerated contours.

CONCLUSIONS

No crystal structure of FLT-3 with an inhibitor is available to assist the design of specific FLT-3 inhibitors. In this study, we used known FLT-3 inhibitors to establish a dual-layer 3D-QSAR model by integrating the pharmacophore, CoMFA, and CoMSIA models. In the 3D-QSAR model, the same training-set inhibitors were used to generate these models. The CoMFA and CoMSIA models were both aligned by using the pharmacophore. The major advantages of the dual-layer 3D-QSAR model are its ability to provide compound database virtual screening and limit the 3D space requirement to fit binding sites of FLT-3 kinase. This dual-layer 3D-QSAR model provided a fragment-based design strategy to discover novel lead inhibitors of FLT-3. We generated 10 pharmacophore hypotheses using 25 FLT-3 inhibitors based on the HypoGen algorithm and used Fischer's test to verify the quality of each hypothesis. All results indicated that Hypo02 could predict high-activity inhibitors of FLT-3. Hypo02 was used to align FLT-3 inhibitors to generate CoMFA and CoMSIA models. On the basis of the Hypo02 alignment rule, the CoMFA and CoMSIA models also had the ability to screen 3D conformations of compound databases. Therefore, the best dual-layer 3D-QSAR model with the highest statistical significance is Hypo02 with CoMFA and CoMSIA models. We discovered nine novel FLT-3 inhibitors based on our model and the fragment compound database. By integrating the pharmacophore,

CoMFA, and CoMSIA models, the dual-layer 3D-QSAR model may provide a new workflow to easily and quickly discover and optimize candidate inhibitors of FLT-3.

ASSOCIATED CONTENT

Supporting Information

Figures S1–S3 show the testing-set inhibitor structures. Table S1 contains actual and predicted IC₅₀ values (nM) of testing-set inhibitors. Table S2 shows the fragment compounds and the nine novel FLT-3 inhibitors. Table S3 shows the predicted activities of the nine novel FLT-3 inhibitors. This material is available free of charge via the Internet at <http://pubs.acs.org>.

AUTHOR INFORMATION

Corresponding Author

*Phone: 886-4-26310631 (C.-Y.T.), 886-4-7232105 ext 3433 (N.-W.H.). Fax: 886-4-26311170 (C.-Y.T.). E-mail: cytang@pu.edu.tw (C.-Y.T.), nady@cc.ncue.edu.tw (N.-W.H.).

Author Contributions

▽ These authors contributed equally to this work

ACKNOWLEDGMENTS

Part of this work was supported by the National Science Council (grant NSC100-2221-E-182-057-MY3, NSC100-2811-E-126-002) and by Chang Gung University (grant UERP-D2A0031). We are grateful to the National Center for High-Performance Computing for computer time and facilities. Kinase KnowledgeBase is the property of Eidogen-Sertanty, Inc. The Sybyl-X 1.0 computation was conducted at Industrial Technology Research Institute, Taiwan.

REFERENCES

- Cools, J.; Mentens, N.; Furet, P.; Fabbro, D.; Clark, J. J.; Griffin, J. D.; Marynen, P.; Gilliland, D. G. Prediction of resistance to small molecule FLT3 inhibitors: implications for molecularly targeted therapy of acute leukemia. *Cancer Res.* **2004**, *64*, 6385–9.
- Furet, P.; Bold, G.; Meyer, T.; Roesel, J.; Guagnano, V. Aromatic interactions with phenylalanine 691 and cysteine 828: a concept for FMS-like tyrosine kinase-3 inhibition. Application to the discovery of a new class of potential antileukemia agents. *J. Med. Chem.* **2006**, *49*, 4451–4.
- Kiyo, H.; Shiotsu, Y.; Ozeki, K.; Yamaji, S.; Kosugi, H.; Umehara, H.; Shimizu, M.; Arai, H.; Ishii, K.; Akinaga, S.; Naoe, T. A novel FLT3 inhibitor FI-700 selectively suppresses the growth of leukemia cells with FLT3 mutations. *Clin. Cancer Res.* **2007**, *13*, 4575–82.
- Markovic, A.; MacKenzie, K. L.; Lock, R. B. FLT-3: a new focus in the understanding of acute leukemia. *Int. J. Biochem. Cell Biol.* **2005**, *37*, 1168–72.
- Parcells, B. W.; Ikeda, A. K.; Simms-Waldrip, T.; Moore, T. B.; Sakamoto, K. M. FMS-like tyrosine kinase 3 in normal hematopoiesis and acute myeloid leukemia. *Stem Cells* **2006**, *24*, 1174–84.
- Fiedler, W.; Serve, H.; Dohner, H.; Schwittay, M.; Ottmann, O. G.; O'Farrell, A. M.; Bello, C. L.; Allred, R.; Manning, W. C.; Cherrington, J. M.; Louie, S. G.; Hong, W.; Brega, N. M.; Massimini, G.; Scigalla, P.; Berdel, W. E.; Hossfeld, D. K. A phase 1 study of SU11248 in the treatment of patients with refractory or resistant acute myeloid leukemia (AML) or not amenable to conventional therapy for the disease. *Blood* **2005**, *105*, 986–93.

- (7) Cheng, Y.; Paz, K. Tandutinib, an oral, small-molecule inhibitor of FLT3 for the treatment of AML and other cancer indications. *IDrugs* **2008**, *11*, 46–56.
- (8) Odgerel, T.; Kikuchi, J.; Wada, T.; Shimizu, R.; Futaki, K.; Kano, Y.; Furukawa, Y. The FLT3 inhibitor PKC412 exerts differential cell cycle effects on leukemic cells depending on the presence of FLT3 mutations. *Oncogene* **2008**, *27*, 3102–10.
- (9) Knapper, S.; Mills, K. I.; Gilkes, A. F.; Austin, S. J.; Walsh, V.; Burnett, A. K. The effects of lestaurtinib (CEP701) and PKC412 on primary AML blasts: the induction of cytotoxicity varies with dependence on FLT3 signaling in both FLT3-mutated and wild-type cases. *Blood* **2006**, *108*, 3494–503.
- (10) Lopes de Menezes, D. E.; Peng, J.; Garrett, E. N.; Louie, S. G.; Lee, S. H.; Wiesmann, M.; Tang, Y.; Shephard, L.; Goldbeck, C.; Oei, Y.; Ye, H.; Aukerman, S. L.; Heise, C. CHIR-258: a potent inhibitor of FLT3 kinase in experimental tumor xenograft models of human acute myelogenous leukemia. *Clin. Cancer Res.* **2005**, *11*, 5281–91.
- (11) Zhou, J.; Khng, J.; Jasinghe, V. J.; Bi, C.; Neo, C. H.; Pan, M.; Poon, L. F.; Xie, Z.; Yu, H.; Yeoh, A. E.; Lu, Y.; Glaser, K. B.; Albert, D. H.; Davidsen, S. K.; Chen, C. S. In vivo activity of ABT-869, a multi-target kinase inhibitor, against acute myeloid leukemia with wild-type FLT3 receptor. *Leuk. Res.* **2008**, *32*, 1091–100.
- (12) Shiotsu, Y.; Kiyoi, H.; Ishikawa, Y.; Tanizaki, R.; Shimizu, M.; Umehara, H.; Ishii, K.; Mori, Y.; Ozeki, K.; Minami, Y.; Abe, A.; Maeda, H.; Akiyama, T.; Kanda, Y.; Sato, Y.; Akinaga, S.; Naoe, T. KW-2449, a novel multikinase inhibitor, suppresses the growth of leukemia cells with FLT3 mutations or T315I-mutated BCR/ABL translocation. *Blood* **2009**, *114*, 1607–17.
- (13) Zarrinkar, P. P.; Gunawardane, R. N.; Cramer, M. D.; Gardner, M. F.; Brigham, D.; Belli, B.; Karaman, M. W.; Pratz, K. W.; Pallares, G.; Chao, Q.; Sprankle, K. G.; Patel, H. K.; Levis, M.; Armstrong, R. C.; James, J.; Bhagwat, S. S. AC220 is a uniquely potent and selective inhibitor of FLT3 for the treatment of acute myeloid leukemia (AML). *Blood* **2009**, *114*, 2984–92.
- (14) Griffith, J.; Black, J.; Faerman, C.; Swenson, L.; Wynn, M.; Lu, F.; Lippke, J.; Saxena, K. The structural basis for autoinhibition of FLT3 by the juxtamembrane domain. *Mol. Cell* **2004**, *13*, 169–78.
- (15) Verstraete, K.; Vandriessche, G.; Januar, M.; Elegheert, J.; Shkumatov, A. V.; Desfosses, A.; Van Craenenbroeck, K.; Svergun, D. I.; Gutsche, I.; Vergauwen, B.; Savvides, S. N. Structural insights into the extracellular assembly of the hematopoietic Flt3 signaling complex. *Blood* **2011**, *118*, 60–8.
- (16) Al-Masri, I. M.; Mohammad, M. K.; Taha, M. O. Discovery of DPP IV inhibitors by pharmacophore modeling and QSAR analysis followed by in silico screening. *ChemMedChem* **2008**, *3*, 1763–79.
- (17) Bharatham, K.; Bharatham, N.; Lee, K. W. Pharmacophore modeling for protein tyrosine phosphatase 1B inhibitors. *Arch. Pharm. Res.* **2007**, *30*, 533–42.
- (18) Boppana, K.; Dubey, P. K.; Jagarlapudi, S. A.; Vadivelan, S.; Rambabu, G. Knowledge based identification of MAO-B selective inhibitors using pharmacophore and structure based virtual screening models. *Eur. J. Med. Chem.* **2009**, *44*, 3584–90.
- (19) Chopra, M.; Gupta, R.; Gupta, S.; Saluja, D. Molecular modeling study on chemically diverse series of cyclooxygenase-2 selective inhibitors: generation of predictive pharmacophore model using catalyst. *J. Mol. Model.* **2008**, *14*, 1087–99.
- (20) Lauria, A.; Ippolito, M.; Fazzari, M.; Tutone, M.; Di Blasi, F.; Mingoia, F.; Almerico, A. M. IKK-beta inhibitors: An analysis of drug-receptor interaction by using Molecular Docking and Pharmacophore 3D-QSAR approaches. *J. Mol. Graphics Modell.* **2010**.
- (21) Mitra, I.; Saha, A.; Roy, K. Pharmacophore mapping of arylamino-substituted benzo[b]thiophenes as free radical scavengers. *J. Mol. Model.* **2010**.
- (22) Ravikumar, M.; Pavan, S.; Bairy, S.; Pramod, A. B.; Sumakanth, M.; Kishore, M.; Sumithra, T. Virtual screening of cathepsin K inhibitors using docking and pharmacophore models. *Chem. Biol. Drug Des.* **2008**, *72*, 79–90.
- (23) Cramer, R. D. 3rd; Patterson, D. E.; Bunce, J. D. Recent advances in comparative molecular field analysis (CoMFA). *Prog. Clin. Biol. Res.* **1989**, *291*, 161–5.
- (24) Cramer, R. D.; Patterson, D. E.; Bunce, J. D. Comparative molecular field analysis (CoMFA). 1. Effect of shape on binding of steroids to carrier proteins. *J. Am. Chem. Soc.* **1988**, *110*, 5959.
- (25) Jiang, Y. K. Molecular docking and 3D-QSAR studies on beta-phenylalanine derivatives as dipeptidyl peptidase IV inhibitors. *J. Mol. Model.* **2010**, *16*, 1239–49.
- (26) Kaur, K.; Talele, T. T. Structure-based CoMFA and CoMSIA study of indolinone inhibitors of PDK1. *J. Comput.-Aided Mol. Des.* **2009**, *23*, 25–36.
- (27) Lei, B. L.; Du, J.; Li, S. Y.; Liu, H. X.; Ren, Y. Y.; Yao, X. J. Comparative molecular field analysis (CoMFA) and comparative molecular similarity indices analysis (CoMSIA) of thiazolone derivatives as hepatitis C virus NSSB polymerase allosteric inhibitors. *J. Comput.-Aided Mol. Des.* **2008**, *22*, 711–725.
- (28) Maitarad, P.; Kamchonwongpaisan, S.; Vanichtanankul, J.; Vilaiwan, T.; Yuthavong, Y.; Hannongbua, S. Interactions between cycloguanil derivatives and wild type and resistance-associated mutant Plasmodium falciparum dihydrofolate reductases. *J. Comput.-Aided Mol. Des.* **2009**, *23*, 241–252.
- (29) Pissurlenkar, R. R. S.; Shaikh, M. S.; Coutinho, E. C. 3D-QSAR studies of Dipeptidyl peptidase IV inhibitors using a docking based alignment. *J. Mol. Model.* **2007**, *13*, 1047–1071.
- (30) Prasanna, S.; Daga, P. R.; Xie, A.; Doerksen, R. J. Glycogen synthase kinase-3 inhibition by 3-anilino-4-phenylmaleimides: insights from 3D-QSAR and docking. *J. Comput.-Aided Mol. Des.* **2009**, *23*, 113–27.
- (31) Sivan, S. K.; Manga, V. Molecular docking and 3D-QSAR studies on triazolinone and pyridazinone, non-nucleoside inhibitor of HIV-1 reverse transcriptase. *J. Mol. Model.* **2010**, *16*, 1169–78.
- (32) Zeng, J.; Liu, G. X.; Tang, Y.; Jiang, H. L. 3D-QSAR studies on fluoropyrrolidine amides as dipeptidyl peptidase IV inhibitors by CoMFA and CoMSIA. *J. Mol. Model.* **2007**, *13*, 993–1000.
- (33) Klebe, G.; Abraham, U.; Mietzner, T. Molecular similarity indices in a comparative analysis (CoMSIA) of drug molecules to correlate and predict their biological activity. *J. Med. Chem.* **1994**, *37*, 4130–46.
- (34) Sprague, P. W. Automated chemical hypothesis generation and database searching with Catalyst(R). *Perspect. Drug Discovery* **1995**, *3*, 1–20.
- (35) Brooks, B. R.; Bruccoleri, R. E.; Olafson, B. D.; States, D. J.; Swaminathan, S.; Karplus, M. CharMM - a Program for Macromolecular Energy, Minimization, and Dynamics Calculations. *J. Comput. Chem.* **1983**, *4*, 187–217.
- (36) Catalyst; Accelrys: San Diego, CA. <http://www.accelrys.com> (accessed Dec. 2011).
- (37) Cramer, R. D.; Bunce, J. D.; Patterson, D. E.; Frank, I. E. Cross-Validation, Bootstrapping, and Partial Least-Squares Compared with Multiple-Regression in Conventional Qsar Studies. *Quant. Struct.-Act. Relat.* **1988**, *7*, 18–25.